ELSEVIER

Surface Science 417 (1998) L1154–L1159

surface science

Surface Science Letters

Kinetic energy effects on the oxidation of Ni(111) using O_2 molecular beams

B.D. Zion, A.T. Hanbicki, S.J. Sibener *

The James Franck Institute and Department of Chemistry, The University of Chicago, 5640 S. Ellis Ave., Chicago, IL 60637, USA

Received 10 August 1998; accepted for publication 9 September 1998

Abstract

The oxidation kinetics of the Ni(111) surface have been quantitatively examined utilizing kinetic energy selected supersonic beams of molecular oxygen. Using in-situ high-resolution electron-energy-loss spectroscopy, we have observed notable differences in the oxidation mechanism for this interface as a function of incident-beam kinetic energy. Exposure of a 300-K surface to a relatively low-energy 60 meV O_2 beam leads to oxidation kinetics that follow an island growth model, qualitatively similar to what is seen with simple ambient gas dosing. In contrast to this, exposure to a relatively high-energy 600 meV O_2 beam yielded a fundamentally different oxidation behavior: the kinetics of oxidation no longer follow an island growth model but rather behave with a Langmuir-like sticking model, implying key differences in the nucleation stage for interface oxidation. Cryogenically cooled Ni(111) could not be oxidized using either of these incident-beam conditions, indicating that the energetic constraints needed to move from oxygen chemisorption to actual metallic oxidation cannot be simply overcome using incident O_2 kinetic energy.

Keywords: Electron-energy-loss spectroscopy; Models of surface kinetics; Molecule–solid reactions; Nickel; Nickel oxides; Oxidation; Oxygen; Surface chemical reaction

Understanding the oxidation behavior of materials is of fundamental importance to both pure and applied science. The oxidation of metals is especially important due to its relevance in the corrosion behavior of real-world systems. Nickel, being one of the most commonly used strategic metals and serving as a model testbed for new concepts of metallic oxidation, has been the focus of many oxidation studies [1–12]. In this letter, we address the oxidation kinetics of the Ni(111) surface utilizing kinetic energy selected supersonic beams of molecular oxygen. Using in-situ high-resolution electron-energy-loss spectroscopy, we have observed notable differences in the oxidation mechanism for this interface as a function of incident-beam kinetic energy.

We have investigated the oxidation of Ni(111) utilizing molecular oxygen beams whose energies span the range from sub- to supra-thermal conditions. Many real-world processes in which metals are used involve high-speed gas–surface collisions, e.g. high-temperature combustion environments, turbines, and high-velocity airframes. The use of relatively high kinetic energy molecular beams provides a means of recreating these extreme conditions in the laboratory, conditions that are inaccessible when using other, less elaborate, ambient dosing conditions typical of previous studies.

* Corresponding author. Fax: +1 773 702 5863; e-mail: s-sibener@uchicago.edu

0039-6028/98/$ – see front matter
PII: S0039-6028(98)00737-7

A great deal is known about the initial stages of oxidation of nickel surfaces. Holloway and Hudson [1,2] characterized three regions of oxygen uptake on a Ni(111) surface exposed to background O_2. The initial uptake proceeds by the facile dissociative chemisorption of oxygen. This is followed by rapid oxidation, and, finally, by a very slow thickening of the saturated nickel oxide overlayer. The behavior of oxygen uptake in this second, or oxidation, regime is particularly sensitive to the presence of nucleation sites for oxide formation. Previous work from our group has shown that electron irradiation can greatly accelerate the formation of such sites, facilitating oxidation [3–5], a phenomenon also seen in other systems [13–17]. In this letter, we show that incident-beam kinetic energy can also lead to significant rate and mechanistic changes in the oxidation of metals. We have found that upon exposure to a collimated, relatively low-kinetic-energy 60 meV molecular beam, oxygen uptake follows the same kinetic mechanism as in the case of background dosing. In contrast, exposure to a relatively high-energy 600 meV O_2 beam yielded fundamentally different oxidation behavior, differing *qualitatively* from previous nickel oxidation models.

Experiments were conducted in a two-level UHV system with a base pressure of 4×10^{-11} Torr. The upper level of the chamber is equipped with an Auger system, low-energy electron diffraction, and a sputter gun for sample preparation and characterization. The lower level (Fig. 1a) contains an LK2000 high-resolution electron-energy-loss spectrometer (HREELS) to monitor and characterize the surface uptake of oxygen, a threefold differentially pumped supersonic beam source, and a quadrupole mass analyzer (QMA) to characterize the beam. The geometry of the lower level is arranged so that the focus of the electron beam spot of the HREELS is coincident with the molecular beam on the crystal surface. The typical resolution of the HREELS was ca. 10 meV FWHM. The molecular beam angle of incidence was set 15° from the surface normal. A Ni(111) sample, described in previous experiments [3–5], was cleaned by repeated cycles of Ar^+ sputtering followed by annealing to 1000 K. The sample temperature was controlled from 120 to 1000 K by cooling

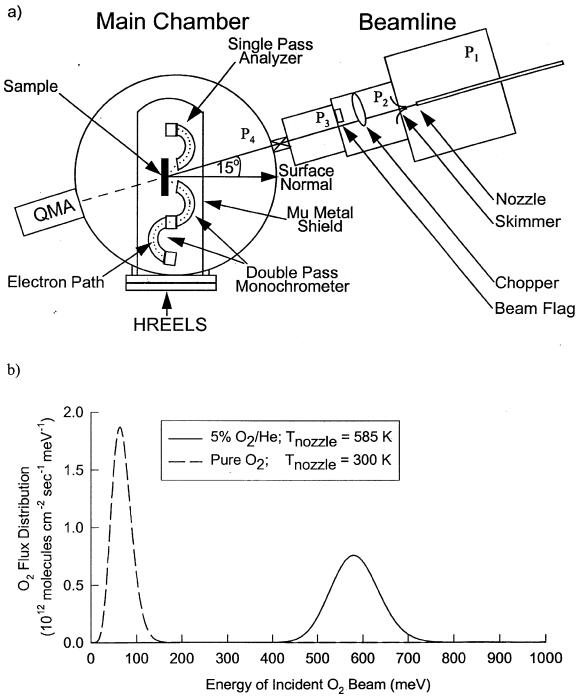

Fig. 1. (a) Schematic of experimental set-up used in this study. The beamline has three differentially pumped regions operating at progressively lower pressures: $P_1 = 10^{-5}$ Torr, $P_2 = 10^{-7}$ Torr, $P_3 = 10^{-9}$ Torr, and, finally, $P_4 = 10^{-10}$ Torr in the main chamber. The beam is incident on the sample at an angle of 15° with respect to the surface normal. The beam spot is coincident with the electron beam of the HREEL spectrometer. The beam nozzle-to-sample distance is 95.6 cm. (b) Energy distributions of the molecular beams used in this study. The total O_2 flux (area under each curve) was the same for each beam condition, 10^{14} molecules cm^{-2} s^{-1}.

with liquid nitrogen or heating with electron bombardment.

The kinetic-energy-dependent oxidation data were obtained by alternately dosing the crystal with a supersonic beam and monitoring the dipole-allowed oxygen vibrations (~65 meV energy loss) in situ with HREELS. Because HREEL spectra were acquired with an electron beam energy of 3.5 eV at a current density of 2 nA cm^{-2}, the probe electrons did not cause any extraneous effects on the oxidation kinetics [4]. While the data were collected, the O_2 beam was blocked by means of a movable flag in the beamline. The dosing times ranged from 5 s to 1 h; data acquisition took about 10 min. Two different beams were used to oxidize

the crystal: one beam, neat O_2 expanded from a room temperature nozzle, had a mean kinetic energy of 60 meV; the other beam, a 5% mixture of O_2 seeded in He, had a mean kinetic energy of 600 meV. Curve fits to time-of-flight data taken with the QMA are shown in Fig. 1b. The beam flux for each condition was determined from time-of-flight data and from the pressure rise in the third differential region of the beamline, P_3, of Fig. 1a. Fluxes for the low- and high-energy beams were adjusted to be equal (beam flux on target 10^{14} molecules $cm^{-2}\,s^{-1}$), simplifying analysis of the comparative kinetics. Each beam was used to oxidize the nickel surface at two different substrate temperatures, 300 K and 120 K.

Fig. 2a shows typical HREEL spectra during dosing. The growth of the Ni–O stretch signal at ~65 meV due to increased oxygen adsorption can be clearly seen. The inset in this figure shows the shifts in the Ni–O peak position as a function of exposure. These shifts are indicative of the different stages of oxygen overlayer formation. Fig. 2b was constructed by plotting $I_{Ni-O}/I_{specular}$, the ratio of the integrated intensity of the Ni–O peak to the integrated specular peak, versus oxygen exposure in units of Langmuirs ($1\,L = 10^{-6}\,Torr \cdot s$). The HREELS intensity ratio is calibrated to monolayers of NiO (Fig. 2b) using the known saturation limit [6] of 3 ML at room temperature. This calibration gives comparable results to the frequently used Auger method of determining concentrations of surface oxygen [4]. The different phases of oxygen uptake described earlier are also indicated in Fig. 2b.

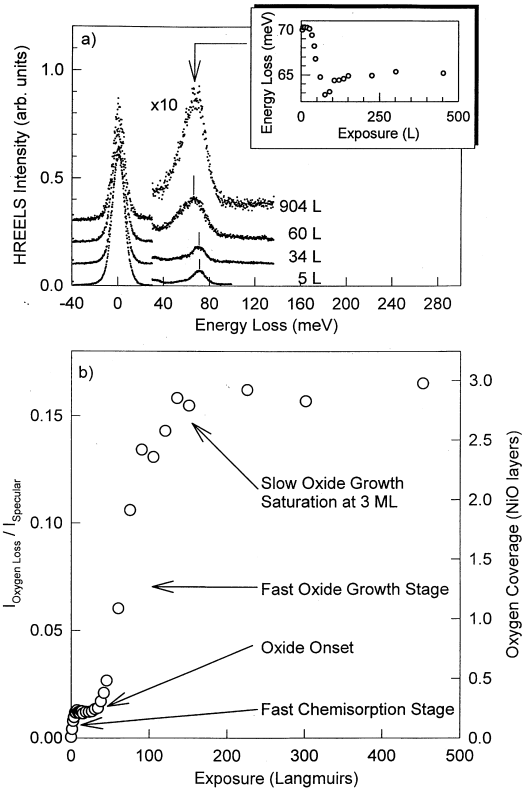

Fig. 2. (a) Illustrative HREEL spectra of Ni(111) during oxygen uptake by beam dosing. The spectra of subsequent doses are offset for clarity. The feature at ~65 meV is the Ni–O stretch, and the inset shows the shift of this peak as a function of exposure. (b) Ratio of the Ni–O peak area to the specular peak area plotted vs. exposure. The characteristic stages of oxygen uptake on Ni(111) are labeled; the HREEL signal is scaled to the absolute oxygen coverage.

Fig. 3 shows the oxygen uptake on Ni(111) versus exposure to both low- and high-kinetic-energy beams with the substrate at either 120 K or 300 K. For all four of these dosing conditions, oxygen uptake has the same behavior below 25 L exposure: rapid chemisorption to ca. 0.25 ML. Beyond 25 L, the behavior of the room and low temperature surfaces deviates significantly. The low-temperature substrate saturates at the chemisorption limit for both beam conditions, a behavior seen previously under exposure to oxygen from background dosing [3–5]. In contrast, the oxygen uptake on the room temperature surfaces continues beyond the chemisorption limit for both beam energies. For both beam conditions, oxidation begins quickly and then slows down near the saturation limit of oxygen uptake. *The shapes of the oxygen uptake curves differ significantly for each dosing energy*.

We first attempted to fit the oxidation data of Fig. 3 for both the high- and low-energy beams with the island growth model of Holloway and Hudson [1], a model originally developed to explain oxidation in the thermal regime using ambient gases. Although the low-energy-beam data are well reproduced by this model, they provide a poor description of the high-energy-beam data. The inability to fit both data sets with

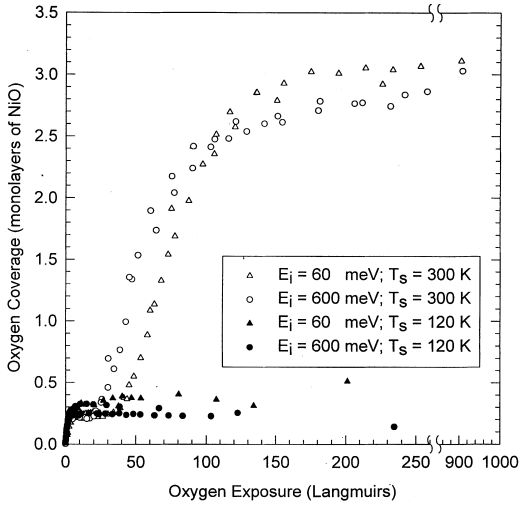

Fig. 3. Oxygen uptake vs. exposure for molecular oxygen beam dosing of Ni(111) under four different conditions. The triangles and circles represent data for oxygen uptake obtained with 60 meV and 600 meV kinetic energy oxygen beams, respectively. The open and filled symbols represent the data for oxygen uptake on the 300 K and 120 K substrate, respectively. The data symbols have been sized to represent the precision of the measurement, consistent also with the scatter of the data set. Note that at low substrate temperatures no oxidation is observed, even with the high-energy beam.

the same kinetic model suggests that qualitatively different mechanisms of oxide growth occur when using low- and high-energy incident fluxes of molecular oxygen. This has led us to develop a new model based on Langmuir kinetics, as discussed below.

We begin this discussion with a brief review of the island growth model. This model assumes lateral growth of oxide islands. Here, growth is dependent on the impingement rate of the oxygen molecules, the initial number of nucleation sites, and a perimeter growth rate constant. An expression for oxygen coverage, Θ, as a function of exposure, Φ, can be derived [1]:

$$\Theta(\Phi)=\Theta_{\mathrm{SAT}}-(\Theta_{\mathrm{SAT}}-\Theta_{\mathrm{CHEMI}}) \times \exp[-K_1 N_0(\Phi-\Phi_0)^2], \text{ for } \Phi>\Phi_0, \quad (1)$$

where Θ_{SAT} is the saturation coverage taken to be 3 ML [4,6], Θ_{CHEMI} is the chemisorbed saturation coverage in ML, K_1 is the island growth rate constant, N_0 is the density of nucleation sites and Φ_0 is the oxide onset exposure (Eq. (1) has been slightly modified from the original used by Holloway and Hudson to include Φ_0 in order to separate the initial chemisorption stage from the ensuing oxidation analysis). Because this expression is valid only in the oxidation growth regime, it is only applicable at exposures greater than Φ_0. Eq. (1) is second-order in exposure due to the dependence of the growth rate on the perimeter of the islands.

A Langmuir growth expression similar to the island growth model can also be derived. The new model now has a first-order dependence in exposure and is based on the assumptions that the oxidation growth rate depends on the impingement rate of the oxygen molecules, a Langmuir surface coverage dependence, and a rate constant. The differential expression for the change in oxide coverage, Θ_{OXIDE}, with change in exposure, Φ, is:

$$\frac{\mathrm{d}\Theta_{\mathrm{OXIDE}}}{\mathrm{d}\Phi}=K_2[(\Theta_{\mathrm{SAT}}-\Theta_{\mathrm{CHEMI}})-\Theta_{\mathrm{OXIDE}}], \quad (2)$$

where K_2 is the Langmuir oxide growth rate constant. Solving this differential equation for oxide coverage as a function of exposure yields:

$$\Theta_{\mathrm{OXIDE}}(\Phi)=(\Theta_{\mathrm{SAT}}-\Theta_{\mathrm{CHEMI}})-\exp[-(K_2\Phi+C)]. \quad (3)$$

The constant of integration, C, can be determined if we stipulate that there is no oxide formed at oxide onset, and that the total coverage of oxygen is the sum of the coverage due to oxide and the coverage due to chemisorbed oxygen. A complete expression can finally be derived for oxygen coverage in the oxidation region using this Langmuir model of growth:

$$\Theta(\Phi)=\Theta_{\mathrm{SAT}}-(\Theta_{\mathrm{SAT}}-\Theta_{\mathrm{CHEM}}) \times \exp[-K_2(\Phi-\Phi_0)], \text{ for } \Phi>\Phi_0. \quad (4)$$

Each model has been used to fit the 60 meV and 600 meV beam data, as shown in Fig. 4. From a least-squares analysis, and indeed as is evident upon inspection, it is determined that the island growth model provides a clear fit to the data obtained with the lower energy beam. To describe the high-energy-beam data, it is necessary to

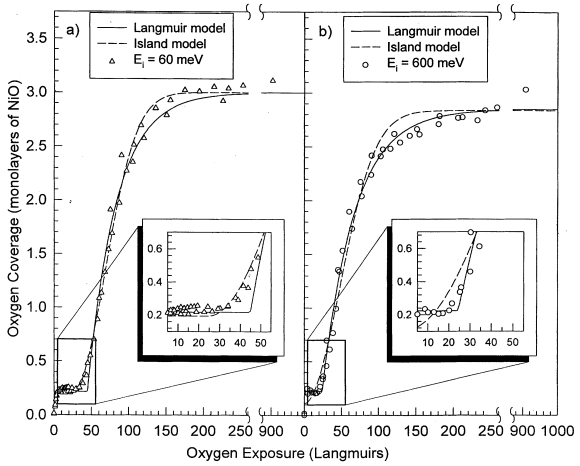

Fig. 4. Best fits of the kinetic models to the oxygen uptake on room temperature Ni(111) for O_2 beams of (a) 60 meV and (b) 600 meV incident kinetic energy. Solid lines represent the Langmuir oxide growth model, and dashed lines represent the island growth model. From these panels, it is clear that the Langmuir model provides a superior fit to the high-energy data, whereas the island growth model is more appropriate for the low-energy data. Insets magnify the oxide onset regime to emphasize this point, as well as highlighting the relative rapidity with which the oxidation onset occurs for the high-energy data.

invoke the Langmuir growth model which more accurately follows the rapid rise at oxide onset and subsequent tail-off in slope near 3 ML coverage.

Table 1 shows the parameters obtained for K_1N_o in this analysis as well as other studies and the value for K_2. The other fit parameters are listed in Table 2. Even though the duration of the chemisorption plateau differs for each condition, the value of Φ_0, the oxide onset point, is nearly the same. Also shown in Table 2 is the square of the value of K_2, which has the same units as K_1N_o and is similar in value.

Table 1
Kinetic model oxidation parameters: values for rate constants

Dosing condition	$T_{substrate}$	K_1N_o	K_2
Low KE[a]	300 K	2.7×10^{-4} L^{-2}	
Backfilling[b]	250 K	3.9×10^{-3} L^{-2}	
	210 K	1.1×10^{-3} L^{-2}	
	180 K	1.6×10^{-4} L^{-2}	
High KE[a]	300 K		2.3×10^{-2} L^{-1}

[a]Present work.
[b]Ref. [5].

Table 2
Kinetic model oxidation parameters: comparison of model-dependent fitting parameters ($T_s = 300$ K)

Parameter	Langmuir High KE	Island growth Low KE
Θ_{SAT}	2.84 ML	3.01 ML
Θ_{CHEMI}	0.25 ML	0.19 ML
Φ_0	24.7 L	24.4 L
K_1N_o	—	2.7×10^{-4} L^{-2}
K_2^2	5.3×10^{-4} L^{-2}	—

One conclusion of this work is found in the comparison of the low-energy beam data and previous work done with simple background dosing of the sample. The data for oxygen uptake on the room temperature substrate under exposure to the low-energy beam are best fitted with the same model originally derived to fit the background dosing data, implying no qualitative changes in the kinetics of nickel oxidation. However, a significant difference in the value of the rate constants for background and beam dosing (Table 1) suggests a quantitative difference in oxide growth under beam exposure. A likely explanation for this difference is that the collimated beam limits the angle of incidence to 15°, whereas background dosing exposes the surface to molecules from all possible angles, with commensurate differences in sticking.

The primary finding from this study is that the kinetics of oxidation actually change functional form under exposure to high-kinetic-energy molecular beams. For low-energy dosing, oxidation is well described by the island growth model; however, the high-kinetic-energy data cannot be fitted with this model. In this regime, the oxidation mechanism follows a kinetic scheme better described by the proposed Langmuir model. In this picture, oxidation may occur anywhere on the exposed surface, not just at island perimeters. This model may also be thought of as oxide nucleation site formation occurring anywhere on the surface. For this model to be true, we require that the rate at which oxygen is incorporated into the new nucleation sites be much faster than the rate at

which oxygen is incorporated into oxide islands. This interpretation implies that there is an energy barrier to oxide nucleation that is overcome by the use of the high-energy incident molecules.

In summary, we have examined the oxidation behavior of Ni(111) during exposure to kinetic energy controlled supersonic beams of molecular oxygen with incident energies spanning the range from 60 to 600 meV. Using in-situ high-resolution electron-energy-loss spectroscopy, we have observed notable differences in the oxidation mechanism for this interface as a function of incident beam kinetic energy. Exposure of a 300 K surface to a relatively low-energy 60 meV O_2 beam leads to oxidation kinetics that follow an island growth model, qualitatively similar to what is seen with simple ambient gas dosing. In contrast to this result, exposure to a relatively high-energy 600 meV O_2 beam yielded fundamentally different oxidation behavior: the kinetics of oxidation no longer follow an island growth model but rather behave with a Langmuir-like sticking model, implying key differences in the nucleation stage for interface oxidation. Cryogenically cooled Ni(111) could not be oxidized using either of these incident beam conditions, indicating that the energetic constraints needed to move from oxygen chemisorption to actual metallic oxidation could not be simply overcome using incident O_2 kinetic energy.

This work is part of an ongoing program that seeks to delineate the dominant mechanistic pathways that are responsible for metallic oxidation in thermal and extreme environments. The results presented herein complement earlier work from our group that showed that electron irradiation can markedly accelerate the oxidation kinetics of metallic surfaces by stimulating the formation of nucleation sites for oxide growth [3–5]. This work is presently being extended to examine synergistic effects during metallic oxidation involving UV photon illumination, as well as the mechanisms responsible for metallic oxidation when beams of atomic oxygen are used as the oxidant.

Acknowledgements

This work was supported by the Air Force Office of Scientific Research, and, in part, by the MRSEC Program of the National Science Foundation at The University of Chicago, Award No. DMR-9400379.

References

[1] P.H. Holloway, J.B. Hudson, Surf. Sci. 43 (1974) 123.
[2] P.H. Holloway, J.B. Hudson, Surf. Sci. 43 (1974) 141.
[3] L. Wei, M.J. Stirniman, S.J. Sibener, Surf. Sci. 329 (1995) L593.
[4] L. Wei, M.J. Stirniman, S.J. Sibener, J. Vac. Sci. Technol. A 13 (1995) 1574.
[5] M.J. Stirniman, L. Wei, S.J. Sibener, J. Chem. Phys. 103 (1995) 451.
[6] P.H. Holloway, J. Vac. Sci. Technol. 18 (1981) 653.
[7] C.R. Brundle, J.Q. Broughton, in: D.A. King, D.P. Woodruff (Eds.), The Chemical Physics of Solid Surfaces and Heterogeneous Catalysis, Vol. 3, Part A, Elsevier, Amsterdam, 1990, pp. 132–388, and references therein.
[8] V.E. Henrich, P.A. Cox, The Surface Science of Metal Oxides, Cambridge University Press, Cambridge, 1994.
[9] A.U. MacRae, Surf. Sci. 1 (1964) 319.
[10] W.-D. Wang, N.J. Wu, P.A. Thiel, J. Chem. Phys. 92 (1990) 2025.
[11] O.L. Warren, P.A. Thiel, J. Chem. Phys. 100 (1994) 659.
[12] J.T. Stuckless, C.E. Wartnaby, N. Al-Sarraf, St.J.B. Dixon-Warren, M. Kovar, D.A. King, J. Chem. Phys. 106 (1997) 2012.
[13] H.D. Ebinger, J.T. Yates Jr., Phys. Rev. B 57 (1998) 1976.
[14] R. Martel, Ph. Avouris, I.-W. Lyo, Science 272 (1996) 385.
[15] J.M. Fontaine, Vide-Couches Minces 38 (1983) 193.
[16] J.M. Rickard, B. Weber, A. Cassuto, J. Chimie Physique 80 (1983) 649.
[17] J. Verhoeven, 3rd Int. Conf. Solid Surf., Vienna, 1977, p. 915.